HHS Public Access

Author manuscript

Dev Cell. Author manuscript; available in PMC 2016 December 21.

Published in final edited form as:

Dev Cell. 2015 December 21; 35(6): 685–697. doi:10.1016/j.devcel.2015.11.018.

Stable force balance between epithelial cells arises from F-actin turnover

Jeanne N. Jodoin[1], **Jonathan S. Coravos**[1], **Soline Chanet**[1], **Claudia G. Vasquez**[1], **Michael Tworoger**[1], **Elena R. Kingston**[1], **Lizabeth A. Perkins**[2], **Norbert Perrimon**[2,3], and **Adam C. Martin**[1]

[1]Department of Biology, Massachusetts Institute of Technology, Cambridge, Massachusetts 02142, USA

[2]Department of Genetics, Harvard Medical School, Boston, MA 02115, USA

[3]Howard Hughes Medical Institute, Boston, MA 02115, USA

Summary

The propagation of force in epithelial tissues requires that the contractile cytoskeletal machinery be stably connected between cells through E-cadherin-containing adherens junctions. In many epithelial tissues the cells' contractile network is positioned at a distance from the junction. However, the mechanism(s) that connect the contractile networks to the adherens junctions, and thus mechanically connect neighboring cells, is poorly understood. Here, we identified the role for F-actin turnover in regulating the contractile cytosketal network's attachment to adherens junctions. Perturbing F-actin turnover via gene depletion or acute drug treatments that slow F-actin turnover destabilized the attachment between the contractile actomyosin network and adherens junctions. Our work identifies a critical role for F-actin turnover in connecting actomyosin to intercellular junctions, defining a dynamic process required for the stability of force balance across intercellular contacts in tissues.

Graphical Abstract

Author Contributions

J.N.J. and A.C.M. designed and performed experiments, analyzed data, and wrote the manuscript. J.S.C., S.C., C.G.V., M.T., and E.R.K designed and performed experiments. L.P. and N.P. generated UAS-shRNA fly lines and performed qPCR analysis.

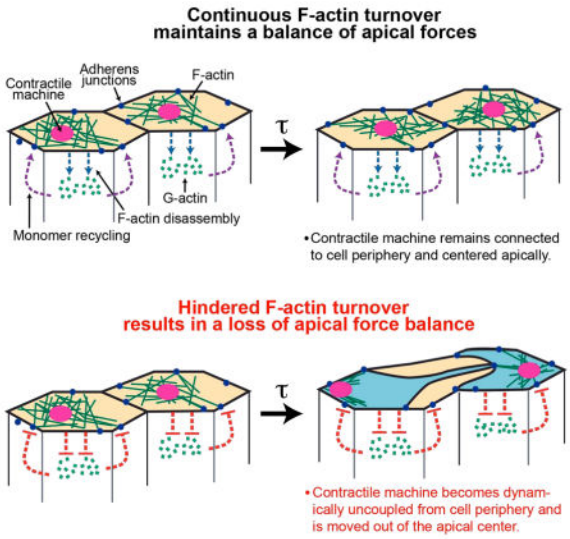

Introduction

During the development of an organism, forces are propagated between mechanically linked cells to alter the form of epithelial tissues (Lecuit et al., 2011). Adherens junctions (AJs) are cell-cell adhesion sites that mechanically couple adjacent cells within a tissue, providing the physical link between cells (Desai et al., 2013; Harris and Tepass, 2010; Takeichi, 2014). Importantly, AJs are attached to a cell's contractile machinery, consisting of actin and myosin (actomyosin) networks and are required for force propagation from one cell to another (Gorfinkiel and Martinez-Arias, 2007; Maitre et al., 2012; Martin et al., 2010). Defects in AJ attachment to the contractile machinery result in failed organ formation (Greene and Copp, 2005; Juriloff and Harris, 2000), loss of cell-cell adhesion (Martin et al., 2010), and are associated with invasiveness of human carcinoma cells (Onder et al., 2008). Despite its importance, how the cell maintains the connection between the contractile machinery and AJs is unclear.

A common outcome of actomyosin network force generation is apical constriction. Apical constriction is a common cell shape change that transforms a columnar-shaped epithelial cell to a wedge shape by reducing its apical surface area (Leptin, 1995; Leptin and Grunewald, 1990). Apical constriction drives the folding of epithelial sheets, such as during the invagination of germ layers in gastrulation (e.g. ventral furrow), and during neural tube closure. Apical constriction in *Drosophila* gastrulation is driven by non-muscle myosin II (MyoII)-mediated contractions of a filamentous actin (F-actin) meshwork spanning the apical surface; MyoII contracts the meshwork centrally on the apical surface, called the medioapical domain (see Figure 4A) (Franke et al., 2005; Martin et al., 2009; Mason et al., 2013). During MyoII-mediated contraction of the apical meshwork, AJ move inward towards the medioapical domain indicating they are connected to the medioapical F-actin meshwork (Martin et al., 2009). Depletion of the AJ components E-cadherin, β–catenin, or α–catenin results in the separation of the MyoII meshwork from the junctional domain, further demonstrating that medioapical actomyosin is connected to AJs (Martin et al., 2010).

Moreover, actomyosin contractility lacking attachments to AJs will generate tension but cannot reduce apical surface area (Martin and Goldstein, 2014; Roh-Johnson et al., 2012). Thus, actomyosin contraction pulls inward on AJs from a distance, highlighting the importance of connecting the contractile machinery to junctional anchor points. Despite the importance of attaching the cell's contractile machine to junctions, the mechanisms that mediate this connection remain poorly understood, though apical constriction and apical tension have often been shown to be associated with stable F-actin or elevated F-actin levels (Haigo et al., 2003; Kinoshita et al., 2008; Lee and Harland, 2007; Spencer et al., 2015; Wu et al., 2014)

Here, we used *Drosophila* gastrulation as a model system to identify mechanisms that promote the attachment of a contractile machine to AJs during apical constriction and tissue folding. We performed a live-embryo imaging RNAi screen to identify actin cytoskeleton genes critical for tissue folding. Our screen revealed a prominent role for genes involved in F-actin turnover in promoting stable force balance between cells. We show that in wild-type cells, the connection between the cell's actomyosin meshwork and AJs is dynamic, with cycles of meshwork release from the AJ followed by its rapid reattachment. Turnover of actin subunits promotes the rapid reattachment of the apical F-actin meshwork to junctions. Slowing the rate of F-actin turnover disrupts this rapid reattachment, which destabilizes the balance of forces across the epithelium and results in neighboring cells dramatically pulling each other back and forth. Our work demonstrates that stable attachment between the contractile machine and AJs during apical constriction requires rapid turnover of the apical F-actin meshwork.

Results

In vivo RNAi screen identified genes required for stable force balance between cells

To determine components of the actomyosin cytoskeleton critical for the attachment of the contractile machinery to AJ during apical constriction, we performed a live-embryo imaging RNAi screen, targeting 50 actin cytoskeleton-related genes. Prior genetic screens identified signaling pathways that promote *Drosophila* gastrulation, but did not identify many components of the cytoskeletal machinery, likely due to their required role during oocyte development (Barrett et al., 1997; Hacker and Perrimon, 1998; Kolsch et al., 2007; Nusslein-Volhard and Wieschaus, 1980; Schupbach and Wieschaus, 1989, 1991). We constructed a library of short-hairpin RNAs (shRNA) targeting individual actin cytoskeleton genes (Table S1), as previously described (Ni et al., 2011). UAS-shRNA expression was driven in flies carrying fluorescent F-actin, MyoII, or plasma membrane markers and the resulting embryos were imaged live (Figure S1A). To overcome the problem that loss of many cytoskeletal genes result in earlier developmental defects or arrest, we tuned the degree of gene depletion to ensure proper embryonic development until gastrulation, allowing us to assess the functions of genes whose depletion would otherwise arrest development prior to tissue invagination (Figures S1B–E). q-PCR and immunoblotting confirmed that UAS-shRNA expression efficiently depleted mRNA transcripts and proteins, respectively, for most targeted genes (Figures S1F and S1G).

In wild-type embryos, tension generated by actomyosin contraction is predominantly directed along the long axis of the ventral furrow (the anterior-posterior axis, A-P axis) (Martin et al., 2010). Despite tension, tracked MyoII structures on the medioapical surface of *control-shRNA (ctl-shRNA)* embryos display very limited back and forth motion, with MyoII structures moving less then 1.0 μm in distance (Figures 1A, 1C, 1E, and S1I). The lack of significant movement in the presence of high tension indicates that contractile forces are to a large extent balanced in wild-type embryos. Our screen revealed that the depletion of genes encoding regulators of F-actin turnover, such as *Drosophila* Profilin (*Chickadee, Chic*) significantly increased the range and velocity in which medioapical MyoII structures moved along the A-P or dorsal-ventral (D-V) axes, indicating a loss in the normal balance of tension along the furrow (Figures 1A, 1D–F, and S1H and S1I). The loss of F-actin turnover phenotype was characterized by the frequent separations in adjacent medioapical actomyosin meshworks that subsequently came back together (Figures 1A, 1B, and Movie S1, *chic-shRNA*). Abnormal movements of medioapical MyoII structures similar to *chic-shRNA* were observed following injection of latrunculin A or B, actin monomer sequestering drugs (Coue et al., 1987), further suggesting that the loss force balance and movement of MyoII structures is due to reduced F-actin turnover (Figure 1G, and Movie S2). Reducing MyoII levels via shRNA-mediated depletion of *Drosophila* Myosin Heavy Chain (*Zipper, Zip)* (Levayer et al., 2015; Vogler et al., 2014) suppressed the velocity of MyoII movement following latrunculin B injection, demonstrating that force generation by MyoII was responsible for the chaotic movement of MyoII structures (Figure 1G).

This phenotype was distinct from the loss of cell-cell adhesion as the depletion of cell adhesion proteins, such as the *Drosophila* Afadin (Canoe, Cno), resulted in a rapid and permanent separation of actomyosin from peripheral anchor points (Sawyer et al., 2009) (Movie S1, *cno-shRNA*). Actomyosin separations in F-actin turnover mutants could be reversed, but when cells pulled back together, they would lose connections with other cells, resulting in a chaotic back and forth movement of medioapical meshworks (Figure 1B). This defect eventually resulted in the loss of cell-cell adhesion and failure to fold the tissue (Figures 1A and 1B, and Movies S1 and S3), suggesting an essential role for actin turnover during apical contractility and epithelial folding.

F-actin disassembly is upregulated in apically constricting cells

During *Drosophila* gastrulation, cells within the ventral region undergo apical constriction to fold the tissue into the embryo. Actomyosin contractility in apically constricting cells is regulated by the ventral-specific expression of the transcription factors *Twist* and *Snail* (Leptin, 1991; Martin et al., 2009). Interestingly, we observed a striking decrease in cortical F-actin levels in ventral cells, that express Twist and Snail, compared to non-ventral cells during apical constriction (Figures 2A and 2B). Phosphorylation of actin depolymerization factor/ Cofilin, (*Drosophila* homolog, *Twinstar*) at Serine 3 has been shown to inhibit its F-actin disassembly activity (Niwa et al., 2002). To determine if Cofilin is differentially regulated in ventral cells, we generated ventralized and lateralized embryos by depleting the ventral fate inhibitor *Spn27a (*using *Spn27a-shRNA)* or the ventral fate inducer *dorsal* (using *dorsal-shRNA*), respectively. The presence of Snail expression around the entire circumference of the embryo confirmed the ventralization of embryos in *Spn27a-shRNA*

embryos (Figure S1J), while the expansion of the lateral marker *Short gastrulation* and the absence of Snail expression confirms the lateralization of *dorsal-shRNA* embryos (Figures 2C and S1K). Cofilin phosphorylation at Serine 3 was lower in ventralized embryos compared to embryos that lack a ventral region, while total Cofilin levels were unchanged (Figures 2C and 2D). To confirm that regulation of Cofilin is responsible for the different F-actin levels in constricting cells, we depleted *Slingshot (Ssh)*, the phosphatase required to remove inhibitory phosphorylation of Cofilin (Niwa et al., 2002). *Ssh* depletion disrupted the ventral-specific decrease in F-actin levels (Figures 2A and 2B). Together, our data demonstrates that Cofilin and F-actin disassembly is activated in ventral cells that undergo apical constriction.

The contractile F-actin meshwork undergoes disassembly to promote apical constriction

Our screen identified two genes that mediate F-actin disassembly, Ssh and *Drosophila Capulet* (*Capt*), as being required for apical constriction. *Capt*, also known as cyclase-associated protein (CAP), promotes actin depolymerization during oocyte development and yeast CAP increases the frequency of Cofilin-mediated F-actin severing *in vitro* (Baum and Perrimon, 2001; Chaudhry et al., 2013). Immunoblotting of *ssh*- and *capt-shRNA* embryo lysates showed a marked increase in phosphorylated Cofilin levels and a decrease in Capt levels, respectively, confirming the shRNA-mediated depletion of these F-actin disassembly factors (Figure S1G). While *ctl-shRNA* embryos exhibit a persistent decrease in apical F-actin levels over time, total apical F-actin levels failed to decrease in *ssh-shRNA* embryos and even initially increased in *capt-shRNA* embryos (Figures 3D and S2A–C). Following an initial increase in *capt-shRNA* embryos, total F-actin levels decreased during late apical constriction (Figure S2C); we speculate that this decrease is due to alternate disassembly mechanisms, such as through MyoII, which has a reported role in F-actin severing (Haviv et al., 2008; Murrell and Gardel, 2012; Vogel et al., 2013; Wilson et al., 2010).

During apical constriction, pulses of MyoII accumulation condense the F-actin meshwork to form a medioapical F-actin focus that is subsequently dispersed (Figure 3A) (Mason et al., 2013; Vasquez et al., 2014). Using three independent methods to disrupt F-actin disassembly, *ssh-shRNA*, *capt-shRNA*, and injection of a small molecule inhibitor of F-actin disassembly, phalloidin, we found that inhibition of F-actin disassembly disrupts medioapical F-actin foci dispersal and F-actin overaccumulates on the apical surface (*ssh*-10/20 embryos, *capt*-12/26 embryos, phalloidin-5/6 embryos) (Figures 3B, 3C, and S2D–H). In addition, depletion of *Ssh* significantly slowed apical constriction compared to *ctl-shRNA* (Figures 3E, S2A and S2B), suggesting that F-actin disassembly is important for the contractile process. Moreover, *ssh-shRNA*, *capt-shRNA*, and phalloidin injected embryos failed to form a ventral furrow (*ssh*-17/27 embryos, *capt*-7/26 embryos, phalloidin-5/6 embryos) (Movie S4). Together, our data show that perturbing F-actin disassembly results in a failure to disperse the contracted medioapical F-actin meshwork (Figure 3F), preventing apical constriction and furrow formation.

The medioapical actomyosin meshwork releases and reattaches to AJs

To investigate the role of recycling actin subunits following F-actin disassembly, we examined apical F-actin dynamics using a fluorescent F-actin marker. During apical

constriction, holes frequently formed in the apical F-actin meshwork and were filled after 46.31 ± 14.5 seconds (Figures 4B and 4C, and Movie S5). Interestingly, live-imaging of embryos expressing F-actin and plasma membrane markers revealed that dynamic meshwork holes corresponded to plasma membrane blebs dynamics, which have been observed in a number of other contractile processes (Charras et al., 2006; Liu et al., 2015; Ruprecht et al., 2015; Sedzinski et al., 2011). We observed that the appearance of F-actin meshwork holes (Figure 4F) often corresponded with bleb protrusion, while F-actin accumulation in the bleb corresponded with plasma membrane retraction. Thus, the formation of F-actin meshwork holes is associated with plasma membrane blebbing, with bleb formation and retraction kinetics similar to blebs in cultured cells (Charras et al., 2006).

Strikingly, live-imaging of E-cadherin, MyoII, or Rho kinase (ROCK) together with F-actin revealed that F-actin meshwork holes preferentially formed between the centrally located contractile machinery and peripheral AJs (Figures 4D, 4E, and S3A). We propose that holes represent the F-actin meshwork releasing and rapidly reattaching to AJs. As an independent indicator of F-actin holes, we found that plasma membrane blebs are statistically enriched between the cell centroid and the junctions (Figures 4G, 4H, S3B, and S3C). These data suggest that F-actin meshwork holes continuously form between the contractile machinery and AJs and are then filled, indicating that the connection between the actomyosin meshwork and the AJs is dynamic during apical constriction.

Actin monomer recycling is essential to rapidly fill F-actin meshwork holes

Because holes in the F-actin meshwork appear and are subsequently filled, we hypothesized that actin monomer recycling was important to rapidly deliver subunits to reassemble the F-actin meshwork in plasma membrane blebs to reestablish the connection between the medioapical actomyosin network and AJs. Our RNAi screen identified genes involved in actin monomer recycling to be required for stable force balance. *Drosophila Chic* and *Ciboulot* (*Cib*) bind globular actin monomers to recycle monomers back to the filamentous state by promoting assembly at F-actin barbed ends; loss of *Chic* or *Cib* results in slower filament turnover (Boquet et al., 2000; Cooley et al., 1992; Verheyen and Cooley, 1994). Holes in the apical F-actin meshwork persisted ~2.6 times longer in *chic- and cib-shRNA* embryos compared to *ctl-shRNA* embryos (Figures S4A and S4B). Moreover, depletion of these actin monomer recycling genes slowed, but did not inhibit the loss of total F-actin levels during apical constriction (Figures S4D–F). Taken together, our data suggest that F-actin disassembly and subsequent monomer recycling are important to disassemble contracted medioapical F-actin networks and to rapidly fill more peripheral F-actin meshwork holes to maintain an apical F-actin network that is attached to AJs (Figure 4B).

F-actin turnover promotes stable coupling of the contractile machinery to AJs

Our screen revealed that slowing F-actin turnover resulted in abnormally high MyoII movement and thus, loss of force balance between cells within a tissue (Figures 1, S1H and S1I). Because MyoII structures exhibited abrupt recoils away from each other (Figures 1A and 1B), we speculated that there was a defect in maintaining connections between mechanical structures. To test whether AJs themselves were compromised, we localized E-cadherin and found that puncta continued to be present at cell-cell interfaces following

depletion of *Ssh*, *Capt*, *Chic* or *Cib*, appeared to be similar to *ctl-shRNA* embryos (N=15 embryos per condition), albeit at a slightly reduced levels (Figure S5A and S5B). Additionally, injection of latrunculin A or B resulted in a loss of force balance similar to *chic-shRNA* and *cib-shRNA* (Figures 1F and 1G, and Movies S1 and S2) without disrupting peripheral E-cadherin localization (Figures S5C–E; 6/6 embryos). Together with the fact that medioapical actomyosin networks can pull back together following chaotic movement due to a force imbalance (Figure 1B), our data suggests that functional AJs exist after disrupting F-actin turnover and that defects in force balance under these conditions are not due to defective AJs.

We next examined whether F-actin turnover facilitates the attachment of the actomyosin meshwork to AJs by filling F-actin meshwork holes. In *ctl-shRNA* embryos, the medioapical actomyosin meshworks remain centrally located on the apical surface and are often connected between cells via MyoII fibers (Martin et al., 2010) (Figure 5A). In contrast, perturbing F-actin turnover via *ssh*, *chic*, or *cib* depletion or injection of small molecule inhibitors resulted in transient separations of actomyosin meshworks of adjacent cells, with medioapical actomyosin in adjacent cells moving away from a shared intercellular contact (*ssh*-11/22 embryos, *chic*-6/15 embryos, *cib*-7/18 embryos, phalloidin-5/6 embryos, latrunculin B-5/7 embryos) (,s 5B-D, S2I and S2J, S5C-E, and Movie S6), resulting in a loss of force balance (Figures 1E, S1H, and S1I). Importantly, phalloidin and latrunculin B were injected immediately prior to apical constriction to acutely inhibit F-actin turnover suggesting that the RNAi phenotypes perturbing F-actin turnover are not due to earlier developmental defects. Additionally, we observed the uncoupled junction move in the opposite direction as MyoII when F-actin turnover was disrupted, whereas junctions were more stably positioned in *ctl-shRNA* embryos (Figure 5E). The movement of the actomyosin meshworks out of the medioapical domain and the opposite motion of the junction, suggests that an imbalance of forces exerted on the actomyosin network could result from a loss of cytoskeletal coupling across a junction.

To determine the nature of this force imbalance, we examined the apical plasma membrane of cells during actomyosin separation. Apical membrane tethers are indicative of a loss of the mechanical linkage on the cytoplasmic side of an AJ connection without the disruption of cell-cell contact (Maitre et al., 2012; Martin et al., 2010). We observed apical membrane separation and membrane tethers during medioapical MyoII displacement events in *ssh*-, *chic*-, and *cib-shRNA* embryos, (Figures 5B″, 5C″, and 5D″). Membrane tethers were also visualized by scanning electron microscopy following *Ssh* depletion (Figures 5H and 5I). This is in contrast to *ctl-shRNA* embryos, which maintain a continuous apical membrane across the tissue (Figure 5A). Together with our visualization of dynamic F-actin meshwork holes, our data suggests that during constriction the apical F-actin meshwork releases some AJs, but rapidly reattaches to AJs via F-actin turnover to maintain force balance and maintain the medioapical localization of the actomyosin network (Figure 5J). Slowing F-actin turnover leads to persistent F-actin meshwork holes (Figure S4B), possible detachment from several AJs, and thus a loss of force balance which results in actomyosin abnormally moving out of the medioapical domain (Figure 5J). Consistent with this interpretation, slowing F-actin disassembly via *capt-shRNA* resulted in the formation of large F-actin holes

and tether structures spanning the gap between F-actin meshworks in adjacent cells (7/26 embryos) (Figures 5F and 5G).

A dynamic response reestablishes force balance between cells

Following separation of medioapical MyoII structures, displaced MyoII foci are re-centered in the medioapical domain, suggesting that the force balance was reestablished (Figures 5B‴, C‴, D‴, 6A–C, and Movie S6). Mechanical connections are reestablished (indicated by the recentering of medioapical MyoII) in *chic-shRNA* and *cib-shRNA* embryos in ~115 seconds, a time-scale similar to the filling of F-actin meshwork holes in these embryos (Figures S4B and S4C). Similarly, we found that laser ablation of apical F-actin networks resulted in actomyosin separation, followed by reestablishment of mechanical connections across the incision (Figures 6D and 6E). Importantly, this response is kinetically distinct from previously described wound healing processes in the early embryo, as MyoII is recruited more rapidly in apically constricting cells than in other cells in the early embryo following laser ablation (Fernandez-Gonzalez and Zallen, 2013). Reestablishing force balance for either *chic-shRNA*, latrunculin B injection, or laser ablated embryos involved MyoII recruitment to the junction between separated actomyosin meshworks prior to the re-centering of the displaced medioapical MyoII structure (Figures 6A–D, S5C, and Movie S7). MyoII recruitment and F-actin assembly at sites of increased tension have been associated with altered signaling pathways due to force-dependent changes in protein interactions (del Rio et al., 2009; Fernandez-Gonzalez et al., 2009; Leerberg et al., 2014; Sawada et al., 2006). Thus, we tested whether activation of signals, such as RhoA-ROCK, serves as a mechanism to repair the loss of force balance.

We observed that ROCK, an upstream activator of MyoII during apical constriction, is recruited to cell interfaces following laser ablation with similar kinetics as MyoII, supporting a hypothesis whereby signaling pathways are activated in response to detachment that recruits MyoII and reestablish force balance (Figures 6E and 6F). To test whether myosin phosphorylation by ROCK was required to recruit myosin to the junction, we investigated whether MyoII uncoupled from its upstream activating kinase could accumulate at junctions following laser ablation. MyoII dynamics (mini-filament assembly and disassembly) is regulated by phosphorylation and dephosphorylation of its regulatory light chain (RLC) via ROCK and myosin phosphatase, respectively (Jordan and Karess, 1997; Karess et al., 1991; Sellers, 1991; Vasquez et al., 2014). RLC phosphomutants locked in a phosphorylated state (RLC-AE) localize to the cortex independent of ROCK activity and are thus uncoupled from upstream regulation (Munjal et al., 2015; Vasquez et al., 2014). Laser ablation of RLC-AE embryos revealed that MyoII uncoupled from its upstream kinase activity does not accumulate at junctions following the severing of MyoII attachment to junctions, where as RLC-TS (*wild-type* RLC) did (Figures 6G and 6H). Moreover, RLC-AE mutants failed to reestablish that connection of MyoII to junctions following laser ablation (Figure 6H), highlighting the requirement of signal activation upstream of MyoII as a mechanism to maintain force balance across the tissue. Taken together, our data suggest that cells respond to a loss of force balance by activating a signaling cascade required to recruit MyoII to the site of detachment to reestablish force balance (Figure 6I).

DISCUSSION

Force propagation across an epithelial tissue requires that cells' contractile machinery remain attached to AJs. Here, we identified a role for F-actin turnover in promoting stable attachment of actomyosin to AJs. Previously, junctional proteins, β-catenin, α-catenin, and *Drosophila* Afadin (cno) were reported to be required at the AJ to link to the contractile machinery. Loss of any of these junctional proteins resulted in irreversible separations of apical actomyosin meshworks (Martin et al., 2010; Roh-Johnson et al., 2012; Sawyer et al., 2009). In contrast, depletion of proteins involved in F-actin turnover resulted in separations of the contractile machine and the cell periphery, followed by the dynamic repair of this separation (Movie S7). In addition to the distinct phenotypes, F-actin turnover proteins exhibit differential subcellular localization. While β-catenin, α-catenin, and Afadin localize predominantly to AJs, tagged and endogenous Capt and Cib localized throughout the apical cytoplasm (Figure S6), consistent with their requirement to rapidly disperse actin throughout the apical domain. Interestingly, Capt enrichment in the apical cytoplasm was specific to apically constricting cells, because Capt became more junctionally localized in non-ventral cells (Figure S6A). The identification of F-actin turnover's role in regulating force balance reveals how a dynamic cellular process promotes stability at the tissue level.

Force balance in a contracting tissue requires F-actin turnover

The actomyosin meshwork must dynamically contract, but remain attached to AJs for cell shape change and to propagate forces across the epithelium (Roh-Johnson et al., 2012). Previous reports suggested that elevated F-actin levels are associated with apical constriction (Haigo et al., 2003; Kinoshita et al., 2008; Lee and Harland, 2007; Spencer et al., 2015; Wu et al., 2014). We demonstrated that in the *Drosophila* embryo, F-actin turnover is upregulated and F-actin levels are downregulated in ventral cells that undergo apical constriction in order to promote force balance and apical constriction. Apical actomyosin meshworks generate force in a wide variety of tissues and organisms (Blanchard et al., 2010; Booth et al., 2014; Lang et al., 2014; Rauzi et al., 2010), our data shows that F-actin turnover is an essential component of this system, which enables forces to be stably propagated between cells.

F-actin turnover reattaches the apical F-actin network to released AJs

We find that F-actin meshwork holes occur between medioapical MyoII structures and peripheral AJs (Figure 7A). Slowing F-actin turnover prolongs the lifetime of F-actin meshwork holes and results in displacement of medioapical contractile networks away from destabilized junctional connections (Figure 7B). Our data supports a loss of the connection between the medioapical actomyosin meshwork and the AJs upon slowing F-actin turnover. Loss of force balance is associated with the formation of plasma membrane tethers between cells, indicating the extracellular attachments remain between cells. This suggests that some part of the connection within the cytoplasm, either the cytoskeletal network itself or its link to the cadherin-catenin complex that make up AJs, is disrupted. Because strong attachment of the cadherin-catenin complex to F-actin requires tension (Buckley et al., 2014), it is possible that formation of an apical F-actin meshwork hole would lead to the release of F-actin bound to cadherin/catenin complexes. Pools of MyoII distinct from the medioapical

MyoII foci and ROCK are recruited to the unattached junctions prior to the repair (Figure 7C), suggesting that ROCK signaling plays an active role in reestablishing force balance; uncoupling MyoII from ROCK signaling inhibits this repair. Interestingly, separations between neighboring cytoskeletal networks were observed in mutants where MyoII was uncoupled from its upstream regulators (Vasquez et al., 2014). Thus, dynamic MyoII recruitment is required in conjunction with rapid F-actin turnover to maintain force balance. Such a dynamic response to loss of attachment is consistent with the proposal that AJs function as mechanical integrators during dynamic tissue movements (Lecuit and Yap, 2015; Leerberg et al., 2014).

F-actin turnover-mediated AJ attachment may play essential roles in other systems

We propose that rapid meshwork turnover is a mechanism for attaching contractile machines to AJs during morphogenesis. In *C. elegans* gastrulation, apical constriction is regulated by a "clutch" that directs contractile motors to engage the cell periphery, leading to apical area reduction (Roh-Johnson et al., 2012). Depletion of Rac, a GTPase implicated in promoting the spatial and temporal distribution of F-actin (Hakeda-Suzuki et al., 2002), resulted in the inability to engage the "clutch". F-actin turnover is an attractive candidate to modulate this clutch as we have shown here that turnover is essential for coupling the contractile machine to AJs. Moreover, loss of Cofilin hinders apical constriction in cultured endothelial cells (Schnittler et al., 2014; Suurna et al., 2006) and mouse neural tube development (Escuin et al., 2015; Grego-Bessa et al., 2015; Juriloff and Harris, 2000). Our work suggests that Cofilin-mediated F-actin turnover in these systems could ensure stable mechanical coupling between contracting cells.

METHODS

Bleb Analysis

Bleb positions were manually annotated by identifying protruding membranes that appeared above cells. A bleb-centroid distance metric was calculated by generating a ray from the geometric centroid through the bleb position, and a third point was defined as the intersection of the ray and the edge of the cell. The bleb-centroid distance metric is the ratio of the bleb-centroid distance to the membrane-centroid distance, where a value of 1 is a position on the cell edge, and a value of 0 is a position on the cell centroid. To evaluate the spatial distribution of the bleb-centroid distance metric, we generated a random set of points and calculated their distances from corresponding cell centroids. Because these distributions were not normal, we compared them using a two-sample Kolmogorov-Smirnov test with an alpha of 0.05.

Image processing and analysis

Image segmentation for quantification of area and F-actin intensities was performed using custom MATLAB software titled EDGE (Embryo Development Geometry Explorer) (Gelbart et al., 2012). A rotationally symmetric Gaussian smoothing filter (kernel = 3 pixels, $\sigma = 0.5$) was applied to raw images. We made maximum intensity projections, summing the top two highest-intensity values. Cell area and integrated fluorescence intensity of Utr::GFP were quantified (Figures 3D, 3E, S2A–C, and S4D–F). Quantifications of F-actin (Utr::GFP)

are from a representative embryo of 2 (*ctl-shRNA*) or 3 (*capt-shRNA*, *ssh-shRNA*, *chic-shRNA*, and *cib-shRNA*) embryos and at least 50 cells were analyzed for each embryo.

Box and whisker plots: red line indicates median. Bottom and top boxes mark the 25th and 75th percentile of the data set, respectively. Black dotted lines mark the lowest and highest value of data set. Red cross indicated outliers that are beyond 1.5 times the inter quartile range of the box edges.

Hole persistence was quantified using FIJI by manually detecting the time from the loss of apical F-actin signal (hole formed) to the reappearance of the signal (filled in). 6 embryos were analyzed per condition and at least 10 holes per embryo. Average hole persistence is presented in Figure S4B. F-actin levels in ventral and lateral regions of the embryos were quantified using FIJI. At least 22 embryos were measured per condition; for each embryo, 2 line scans crossing 5 cells were placed in the ventral or lateral region and cortical F-actin intensity was measured for each cell. The average intensity for each measurement is presented in Figure 2B. Error bars represent SD. FIJI line scans were used to measure MyoII recruitment (sqh::CH or sqh::GFP) and ROCK signals (ubi-GFP::ROCK) prior to and following laser ablation. Data represents the average of 4 embryos, at least 3 MyoII/ROCK foci per embryo. The average timing of protein recruitment is presented in Figures 6F and 6G. Error bars represent SEM. Junctional and medioapical E-cadherin levels were measured using FIJI. E-cadherin intensity (AU) was measured within a 0.5 μm^2 square at the junction and medioapical domain in image cross-sections. Data represents 50 cells from 10 embryos (*ctl-shRNA)*, 22 cells from 9 embryos (*capt-shRNA*), 30 cells from 8 embryos (*chic-shRNA*), 44 cells from 10 embryos (*cib-shRNA*), and 32 cells from 6 embryos (*ssh-shRNA*). The average ratio of junctional to medioapical E-cadherin is presented in Figure S5B. Force balance was measured in two ways: (1) MyoII movement was measured by manually tracking discrete MyoII structures using MTrackJ plugin in FIJI. We tracked large medioapical myosin structures, which were unambiguously identified and similarly apparent when comparing wild-type and F-actin gene depletions. The distance (μm) in which a MyoII structure persisted in the A-P or D-V axis was measured and is presented in Figures 1E, S1H, and S1I. Representative tracks shown in Figures 1C and 1D were plotted using MATLAB. Data represents ~20 MyoII structures from 2 embryos for each condition. (2) MyoII velocity was measured by manually calculating the distance discrete MyoII structures move over a specified time. The average velocity is presented in Figures 1F and 1G. Data represents 20 MyoII structures from 3 embryos for each condition.

See Supplemental Methods for information regarding fly stocks, microscopy, image processing, laser ablation, immunofluorescence, immunoblotting, RNA isolation, reverse transcription, real-time qPCR, shRNA line generation, Generation of *GFP::Capt*, and drug injections.

Supplementary Material

Refer to Web version on PubMed Central for supplementary material.

Acknowledgments

We thank B. Baum, T. Préat, Y. Jan, S. Wasserman, M. Biggins, S. Carreno, E. Wieschaus and the Bloomington Stock Center for fly stocks and antibodies used in this study. Additionally, we thank T. Orr-Weaver, A. Sokac, I. Cheeseman, M. Broadus, and members of the Martin laboratory for their helpful comments and discussion on this manuscript. We additionally thank Coleen Kelley and Rong Tao for technical help. This work was supported by grants from the National Institute of General Medical Sciences: F32GM113425 to J.N.J., R01GM084947 to N.P., and R01GM105984 to A.C.M. N.P. is an investigator of the Howard Hughes Medical Institute. The authors declare no competing financial interests.

References

Barrett K, Leptin M, Settleman J. The Rho GTPase and a putative RhoGEF mediate a signaling pathway for the cell shape changes in Drosophila gastrulation. Cell. 1997; 91:905–915. [PubMed: 9428514]

Baum B, Perrimon N. Spatial control of the actin cytoskeleton in Drosophila epithelial cells. Nature cell biology. 2001; 3:883–890. [PubMed: 11584269]

Blanchard GB, Murugesu S, Adams RJ, Martinez-Arias A, Gorfinkiel N. Cytoskeletal dynamics and supracellular organisation of cell shape fluctuations during dorsal closure. Development. 2010; 137:2743–2752. [PubMed: 20663818]

Booth AJ, Blanchard GB, Adams RJ, Roper K. A dynamic microtubule cytoskeleton directs medial actomyosin function during tube formation. Developmental cell. 2014; 29:562–576. [PubMed: 24914560]

Boquet I, Boujemaa R, Carlier MF, Preat T. Ciboulot regulates actin assembly during Drosophila brain metamorphosis. Cell. 2000; 102:797–808. [PubMed: 11030623]

Buckley CD, Tan J, Anderson KL, Hanein D, Volkmann N, Weis WI, Nelson WJ, Dunn AR. Cell adhesion. The minimal cadherin-catenin complex binds to actin filaments under force. Science. 2014; 346:1254211. [PubMed: 25359979]

Charras GT, Hu CK, Coughlin M, Mitchison TJ. Reassembly of contractile actin cortex in cell blebs. The Journal of cell biology. 2006; 175:477–490. [PubMed: 17088428]

Chaudhry F, Breitsprecher D, Little K, Sharov G, Sokolova O, Goode BL. Srv2/cyclase-associated protein forms hexameric shurikens that directly catalyze actin filament severing by cofilin. Molecular biology of the cell. 2013; 24:31–41. [PubMed: 23135996]

Cooley L, Verheyen E, Ayers K. chickadee encodes a profilin required for intercellular cytoplasm transport during Drosophila oogenesis. Cell. 1992; 69:173–184. [PubMed: 1339308]

Coue M, Brenner SL, Spector I, Korn ED. Inhibition of actin polymerization by latrunculin A. FEBS letters. 1987; 213:316–318. [PubMed: 3556584]

del Rio A, Perez-Jimenez R, Liu R, Roca-Cusachs P, Fernandez JM, Sheetz MP. Stretching single talin rod molecules activates vinculin binding. Science. 2009; 323:638–641. [PubMed: 19179532]

Desai R, Sarpal R, Ishiyama N, Pellikka M, Ikura M, Tepass U. Monomeric alpha-catenin links cadherin to the actin cytoskeleton. Nature cell biology. 2013; 15:261–273. [PubMed: 23417122]

Escuin S, Vernay B, Savery D, Gurniak CB, Witke W, Greene ND, Copp AJ. Rho kinase-dependent actin turnover and actomyosin disassembly are necessary for mouse spinal neural tube closure. Journal of cell science. 2015

Fernandez-Gonzalez R, de Simoes SM, Roper JC, Eaton S, Zallen JA. Myosin II dynamics are regulated by tension in intercalating cells. Developmental cell. 2009; 17:736–743. [PubMed: 19879198]

Fernandez-Gonzalez R, Zallen JA. Wounded cells drive rapid epidermal repair in the early Drosophila embryo. Molecular biology of the cell. 2013; 24:3227–3237. [PubMed: 23985320]

Franke JD, Montague RA, Kiehart DP. Nonmuscle myosin II generates forces that transmit tension and drive contraction in multiple tissues during dorsal closure. Current biology : CB. 2005; 15:2208–2221. [PubMed: 16360683]

Gorfinkiel N, Martinez-Arias A. Requirements for adherens junction components in the interaction between epithelial tissues during dorsal closure in Drosophila. Journal of cell science. 2007; 120:3289–3298. [PubMed: 17878238]

Greene ND, Copp AJ. Mouse models of neural tube defects: investigating preventive mechanisms. American journal of medical genetics Part C, Seminars in medical genetics. 2005; 135C:31–41.

Grego-Bessa J, Hildebrand J, Anderson KV. Morphogenesis of the mouse neural plate depends on distinct roles of cofilin 1 in apical and basal epithelial domains. Development. 2015; 142:1305–1314. [PubMed: 25742799]

Hacker U, Perrimon N. DRhoGEF2 encodes a member of the Dbl family of oncogenes and controls cell shape changes during gastrulation in Drosophila. Genes & development. 1998; 12:274–284. [PubMed: 9436986]

Haigo SL, Hildebrand JD, Harland RM, Wallingford JB. Shroom induces apical constriction and is required for hingepoint formation during neural tube closure. Current biology : CB. 2003; 13:2125–2137. [PubMed: 14680628]

Hakeda-Suzuki S, Ng J, Tzu J, Dietzl G, Sun Y, Harms M, Nardine T, Luo L, Dickson BJ. Rac function and regulation during Drosophila development. Nature. 2002; 416:438–442. [PubMed: 11919634]

Harris TJ, Tepass U. Adherens junctions: from molecules to morphogenesis. Nature reviews Molecular cell biology. 2010; 11:502–514. [PubMed: 20571587]

Haviv L, Gillo D, Backouche F, Bernheim-Groswasser A. A cytoskeletal demolition worker: myosin II acts as an actin depolymerization agent. Journal of molecular biology. 2008; 375:325–330. [PubMed: 18021803]

Jordan P, Karess R. Myosin light chain-activating phosphorylation sites are required for oogenesis in Drosophila. The Journal of cell biology. 1997; 139:1805–1819. [PubMed: 9412474]

Juriloff DM, Harris MJ. Mouse models for neural tube closure defects. Human molecular genetics. 2000; 9:993–1000. [PubMed: 10767323]

Karess RE, Chang XJ, Edwards KA, Kulkarni S, Aguilera I, Kiehart DP. The regulatory light chain of nonmuscle myosin is encoded by spaghetti-squash, a gene required for cytokinesis in Drosophila. Cell. 1991; 65:1177–1189. [PubMed: 1905980]

Kinoshita N, Sasai N, Misaki K, Yonemura S. Apical accumulation of Rho in the neural plate is important for neural plate cell shape change and neural tube formation. Molecular biology of the cell. 2008; 19:2289–2299. [PubMed: 18337466]

Kolsch V, Seher T, Fernandez-Ballester GJ, Serrano L, Leptin M. Control of Drosophila gastrulation by apical localization of adherens junctions and RhoGEF2. Science. 2007; 315:384–386. [PubMed: 17234948]

Lang RA, Herman K, Reynolds AB, Hildebrand JD, Plageman TF Jr. p120-catenin-dependent junctional recruitment of Shroom3 is required for apical constriction during lens pit morphogenesis. Development. 2014; 141:3177–3187. [PubMed: 25038041]

Lecuit T, Lenne PF, Munro E. Force generation, transmission, and integration during cell and tissue morphogenesis. Annual review of cell and developmental biology. 2011; 27:157–184.

Lecuit T, Yap AS. E-cadherin junctions as active mechanical integrators in tissue dynamics. Nature cell biology. 2015; 17:533–539. [PubMed: 25925582]

Lee JY, Harland RM. Actomyosin contractility and microtubules drive apical constriction in Xenopus bottle cells. Developmental biology. 2007; 311:40–52. [PubMed: 17868669]

Leerberg JM, Gomez GA, Verma S, Moussa EJ, Wu SK, Priya R, Hoffman BD, Grashoff C, Schwartz MA, Yap AS. Tension-sensitive actin assembly supports contractility at the epithelial zonula adherens. Current biology : CB. 2014; 24:1689–1699. [PubMed: 25065757]

Leptin M. twist and snail as positive and negative regulators during Drosophila mesoderm development. Genes & development. 1991; 5:1568–1576. [PubMed: 1884999]

Leptin M. Drosophila gastrulation: from pattern formation to morphogenesis. Annual review of cell and developmental biology. 1995; 11:189–212.

Leptin M, Grunewald B. Cell shape changes during gastrulation in Drosophila. Development. 1990; 110:73–84. [PubMed: 2081472]

Levayer R, Hauert B, Moreno E. Cell mixing induced by myc is required for competitive tissue invasion and destruction. Nature. 2015; 524:476–480. [PubMed: 26287461]

Liu YJ, Le Berre M, Lautenschlaeger F, Maiuri P, Callan-Jones A, Heuze M, Takaki T, Voituriez R, Piel M. Confinement and low adhesion induce fast amoeboid migration of slow mesenchymal cells. Cell. 2015; 160:659–672. [PubMed: 25679760]

Maitre JL, Berthoumieux H, Krens SF, Salbreux G, Julicher F, Paluch E, Heisenberg CP. Adhesion functions in cell sorting by mechanically coupling the cortices of adhering cells. Science. 2012; 338:253–256. [PubMed: 22923438]

Martin AC, Gelbart M, Fernandez-Gonzalez R, Kaschube M, Wieschaus EF. Integration of contractile forces during tissue invagination. The Journal of cell biology. 2010; 188:735–749. [PubMed: 20194639]

Martin AC, Goldstein B. Apical constriction: themes and variations on a cellular mechanism driving morphogenesis. Development. 2014; 141:1987–1998. [PubMed: 24803648]

Martin AC, Kaschube M, Wieschaus EF. Pulsed contractions of an actin-myosin network drive apical constriction. Nature. 2009; 457:495–499. [PubMed: 19029882]

Mason FM, Tworoger M, Martin AC. Apical domain polarization localizes actin-myosin activity to drive ratchet-like apical constriction. Nature cell biology. 2013; 15:926–936. [PubMed: 23831726]

Munjal A, Philippe JM, Munro E, Lecuit T. A self-organized biomechanical network drives shape changes during tissue morphogenesis. Nature. 2015; 524:351–355. [PubMed: 26214737]

Murrell MP, Gardel ML. F-actin buckling coordinates contractility and severing in a biomimetic actomyosin cortex. Proceedings of the National Academy of Sciences of the United States of America. 2012; 109:20820–20825. [PubMed: 23213249]

Ni JQ, Zhou R, Czech B, Liu LP, Holderbaum L, Yang-Zhou D, Shim HS, Tao R, Handler D, Karpowicz P, et al. A genome-scale shRNA resource for transgenic RNAi in Drosophila. Nature methods. 2011; 8:405–407. [PubMed: 21460824]

Niwa R, Nagata-Ohashi K, Takeichi M, Mizuno K, Uemura T. Control of actin reorganization by Slingshot, a family of phosphatases that dephosphorylate ADF/cofilin. Cell. 2002; 108:233–246. [PubMed: 11832213]

Nusslein-Volhard C, Wieschaus E. Mutations affecting segment number and polarity in Drosophila. Nature. 1980; 287:795–801. [PubMed: 6776413]

Onder TT, Gupta PB, Mani SA, Yang J, Lander ES, Weinberg RA. Loss of E-cadherin promotes metastasis via multiple downstream transcriptional pathways. Cancer research. 2008; 68:3645–3654. [PubMed: 18483246]

Rauzi M, Lenne PF, Lecuit T. Planar polarized actomyosin contractile flows control epithelial junction remodelling. Nature. 2010; 468:1110–1114. [PubMed: 21068726]

Roh-Johnson M, Shemer G, Higgins CD, McClellan JH, Werts AD, Tulu US, Gao L, Betzig E, Kiehart DP, Goldstein B. Triggering a cell shape change by exploiting preexisting actomyosin contractions. Science. 2012; 335:1232–1235. [PubMed: 22323741]

Ruprecht V, Wieser S, Callan-Jones A, Smutny M, Morita H, Sako K, Barone V, Ritsch-Marte M, Sixt M, Voituriez R, et al. Cortical contractility triggers a stochastic switch to fast amoeboid cell motility. Cell. 2015; 160:673–685. [PubMed: 25679761]

Sawada Y, Tamada M, Dubin-Thaler BJ, Cherniavskaya O, Sakai R, Tanaka S, Sheetz MP. Force sensing by mechanical extension of the Src family kinase substrate p130Cas. Cell. 2006; 127:1015–1026. [PubMed: 17129785]

Sawyer JK, Harris NJ, Slep KC, Gaul U, Peifer M. The Drosophila afadin homologue Canoe regulates linkage of the actin cytoskeleton to adherens junctions during apical constriction. The Journal of cell biology. 2009; 186:57–73. [PubMed: 19596848]

Schnittler H, Taha M, Schnittler MO, Taha AA, Lindemann N, Seebach J. Actin filament dynamics and endothelial cell junctions: the Ying and Yang between stabilization and motion. Cell and tissue research. 2014; 355:529–543. [PubMed: 24643678]

Schupbach T, Wieschaus E. Female sterile mutations on the second chromosome of Drosophila melanogaster. I. Maternal effect mutations. Genetics. 1989; 121:101–117. [PubMed: 2492966]

Schupbach T, Wieschaus E. Female sterile mutations on the second chromosome of Drosophila melanogaster. II. Mutations blocking oogenesis or altering egg morphology. Genetics. 1991; 129:1119–1136. [PubMed: 1783295]

Sedzinski J, Biro M, Oswald A, Tinevez JY, Salbreux G, Paluch E. Polar actomyosin contractility destabilizes the position of the cytokinetic furrow. Nature. 2011; 476:462–466. [PubMed: 21822289]

Sellers JR. Regulation of cytoplasmic and smooth muscle myosin. Current opinion in cell biology. 1991; 3:98–104. [PubMed: 1854490]

Spencer AK, Siddiqui BA, Thomas JH. Cell shape change and invagination of the cephalic furrow involves reorganization of F-actin. Developmental biology. 2015

Suurna MV, Ashworth SL, Hosford M, Sandoval RM, Wean SE, Shah BM, Bamburg JR, Molitoris BA. Cofilin mediates ATP depletion-induced endothelial cell actin alterations. American journal of physiology Renal physiology. 2006; 290:F1398–1407. [PubMed: 16434575]

Takeichi M. Dynamic contacts: rearranging adherens junctions to drive epithelial remodelling. Nature reviews Molecular cell biology. 2014; 15:397–410. [PubMed: 24824068]

Vasquez CG, Tworoger M, Martin AC. Dynamic myosin phosphorylation regulates contractile pulses and tissue integrity during epithelial morphogenesis. The Journal of cell biology. 2014; 206:435–450. [PubMed: 25092658]

Verheyen EM, Cooley L. Profilin mutations disrupt multiple actin-dependent processes during Drosophila development. Development. 1994; 120:717–728. [PubMed: 7600952]

Vogel SK, Petrasek Z, Heinemann F, Schwille P. Myosin motors fragment and compact membrane-bound actin filaments. eLife. 2013; 2:e00116. [PubMed: 23326639]

Vogler G, Liu J, Iafe TW, Migh E, Mihaly J, Bodmer R. Cdc42 and formin activity control non-muscle myosin dynamics during Drosophila heart morphogenesis. The Journal of cell biology. 2014; 206:909–922. [PubMed: 25267295]

Wilson CA, Tsuchida MA, Allen GM, Barnhart EL, Applegate KT, Yam PT, Ji L, Keren K, Danuser G, Theriot JA. Myosin II contributes to cell-scale actin network treadmilling through network disassembly. Nature. 2010; 465:373–377. [PubMed: 20485438]

Wu SK, Gomez GA, Michael M, Verma S, Cox HL, Lefevre JG, Parton RG, Hamilton NA, Neufeld Z, Yap AS. Cortical F-actin stabilization generates apical-lateral patterns of junctional contractility that integrate cells into epithelia. Nature cell biology. 2014; 16:167–178. [PubMed: 24413434]

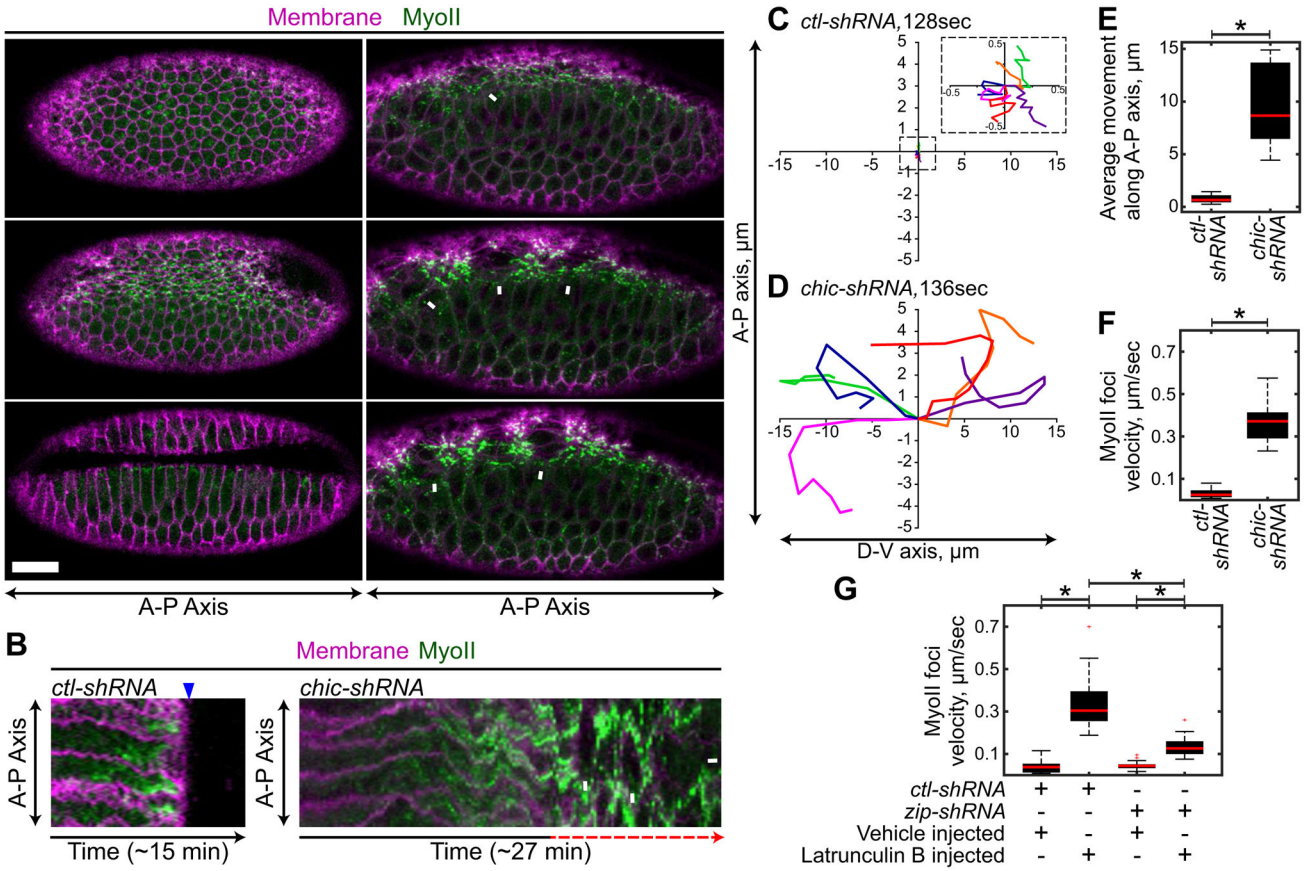

Figure 1. F-actin turnover is required for force balance between cells of a contracting tissue

(A and B) Indicated shRNA expression driven by a GAL4 drivers expressing Sqh::GFP (MyoII) and Gap43::CHFP (membrane). White arrows indicate MyoII separations. (A) Representative time-lapse images of MyoII and membrane. Scale bar, 20µm. (B) Kymographs of MyoII and membrane signals using a line drawn along axis of the furrow. Red dotted arrow indicates back and forth MyoII movement, blue arrowhead indicates tissue invagination. (C–D) Representative tracks of MyoII foci movement following *ctl* (C) or *chic* (D) depletion. Time indicates the length of track. (E) Box and whisker plot of the distance MyoII moves along A-P axis following indicated gene depletion. **p*<0.00001. Data represents n=2 embryos, 10 MyoII structures per condition. (F) Box and whisker plot of MyoII structure velocity following indicated gene depletion. **p*<0.00001. Data represents n=3 embryos, 20 MyoII structures per condition. (G) Box and whisker plot of MyoII structure velocity following indicated gene depletion and injection. **p*<0.00001. Data represents n=3 embryos, 20 MyoII structures per condition. See also Figures S1, Tables S1, and Movies S1–S3.

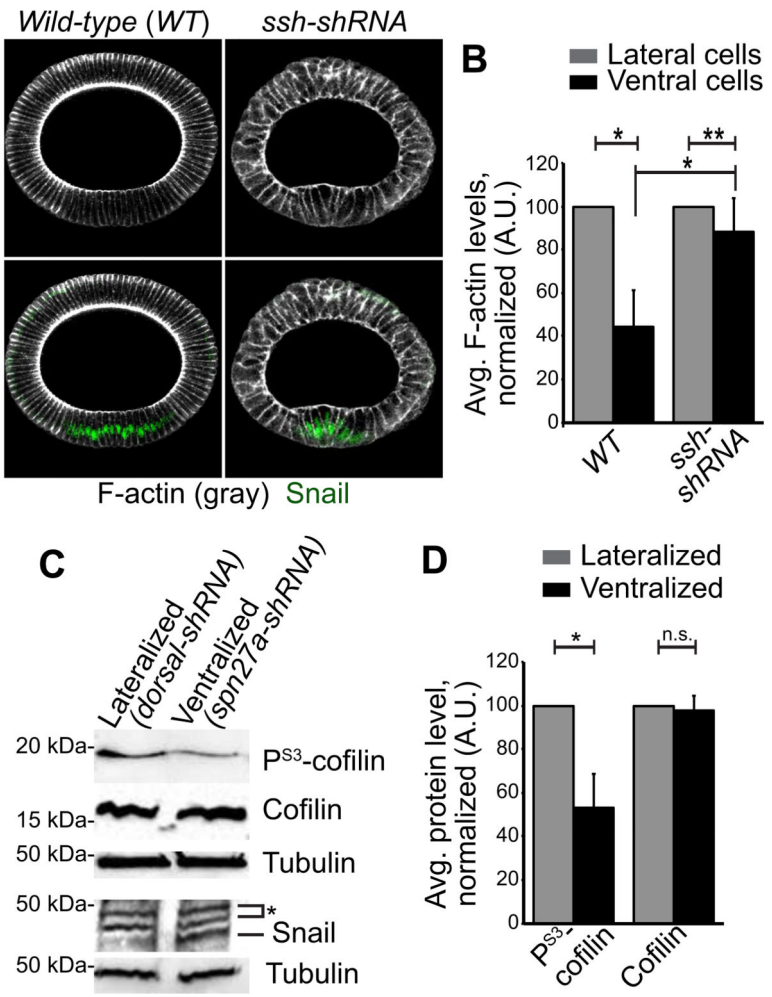

Figure 2. F-actin turnover is upregulated in apically constricting cells

(A) Representative cross-sections stained for phalloidin (F-actin, gray) and Snail (ventral region, green) following indicated gene depletion. Scale bar, 20μm. (B) Cortical F-actin levels in ventral cells, normalized to non-ventral cell F-actin levels for each condition. n=22 embryos per condition. *p<0.0001, **p<0.01. Error bars represent SD. (C) Lysates from *Spn27a-shRNA* (expanded ventral region) and *dorsal-shRNA* (lacking ventral region) probed for indicated antibodies. Asterisk indicates non-specific bands. Tubulin used as a loading control. (D) Average Phospho-Cofilin and total Cofilin levels in ventralized embryo lysates compared to lateralized embryo lysates, normalized to lateral cell levels. Data represent n=3 experiments. *p<0.0001, n.s. is not significant. Error bars represent SD. See also Figure S1.

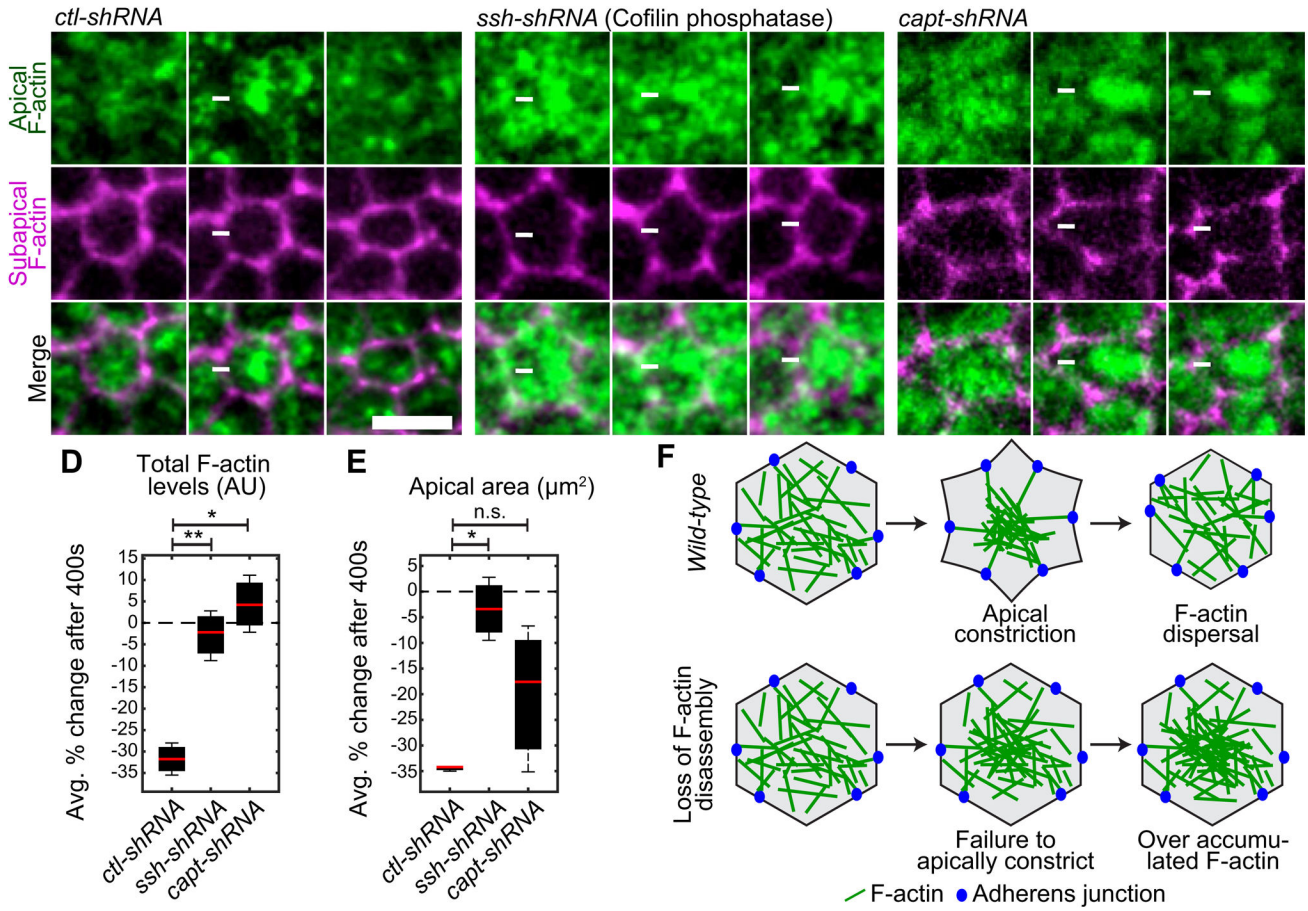

Figure 3. F-actin disassembly is required to disperse medioapical F-actin foci

(A–C) Time-lapse images of representative cells from embryos expressing indicated UAS-shRNA and Utr::GFP (F-actin) following indicated gene depletion. White arrow indicates medioapical focus. Scale bars; 5μm. Box and whisker plot of the percent change in total apical F-actin level (D) and apical area reduction (E) 400 seconds after apical constriction onset. Data represents n=3 embryos, ~50 cells per embryo for each condition. *p<0.0001, **p<0.001. (F) Schematic of the requirement for F-actin disassembly for F-actin foci remodeling during apical constriction. See also Figure S2 and Movie S4.

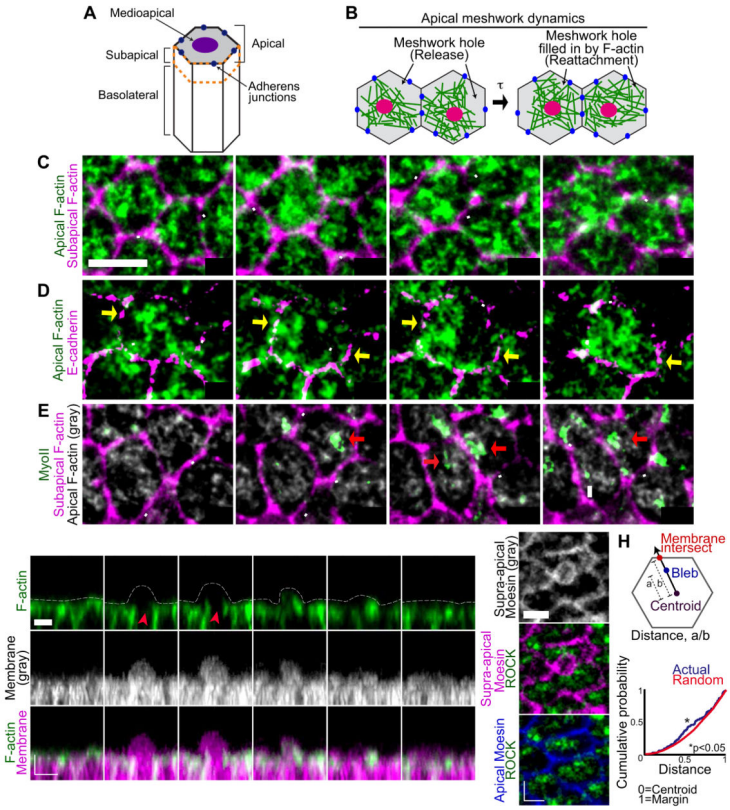

Figure 4. Medioapical actomyosin releases and reattaches to AJs during apical constriction

(A) Diagram of ventral furrow cell domains. (B) Schematic of apical F-actin dynamics during apical constriction. Holes dynamically form in the F-actin meshwork between the contractile machinery (magenta circles) and AJs (blue circles). Time-lapse images of live *ctl-shRNA* embryos expressing (C) Utr::GFP (apical and subapical F-actin), (D) Utr::CHFP (F-actin) and ubi-E-cadherin::GFP (E-cadherin), or (E) Utr::CHFP (apical and subapical F-actin) and Sqh::GFP (MyoII). White arrowheads indicate F-actin meshwork holes, yellow arrows indicate AJs, and red arrows indicate contractile machinery. (F) Time-lapse images of ventral cells in cross-section expressing Utr::Venus (F-actin) and Gap43::CHFP (membrane). Red arrow indicates apical F-actin depletion, white arrowhead indicates bleb protrusion. Dotted white line shows membrane position. (G) Representative images of fixed embryos expressing ubi-GFP::ROCK (ROCK) and stained for Moesin. (H) Quantitative analysis of bleb position on apical surface. Data represents n=3, ~20 blebs per embryo. *$p <$ 0.05. Scale bars; 5μm. See also Figure S3 and Movie S5.

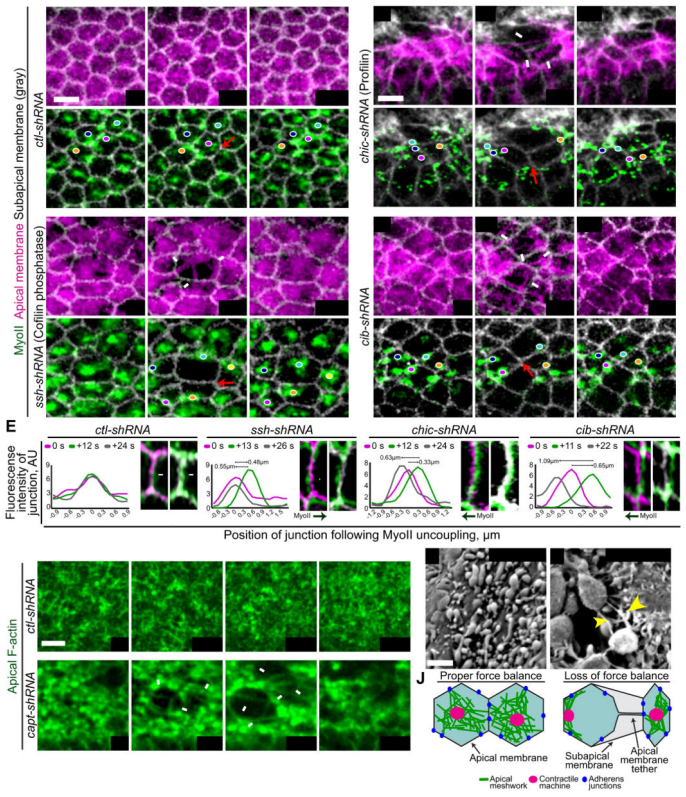

Figure 5. F-actin turnover is required to connect the contractile machinery to AJs

(A–D) Time-lapse images of representative cell groups from embryos expressing the indicated UAS-shRNA, Sqh::GFP (MyoII), and Gap43::CHFP (apical and subapical membrane). Colored dots track MyoII foci. White arrows indicate membrane tethers, red arrows indicate junction analyzed in E. (E) Line graphs show the position of junctions at time points following MyoII displacement. Images are zoomed in junctions from A–D. White arrowheads indicate junction movement, black arrows indicate direction of MyoII displacement. (F and G) Time-lapse images of representative cells from embryos expressing indicated UAS-shRNA and Utr::GFP (F-actin) following indicated gene depletion. White arrows indicate F-actin tethers. (H–I) Membrane tethers (yellow arrows) observed by scanning electron microscopy in *ssh-shRNA* embryos. Scale bars; 5µm. (J) Schematic of how loss of force balance results in the medioapical MyoII displacement and plasma membrane tethers. See also Figures S4 and Movies S6.

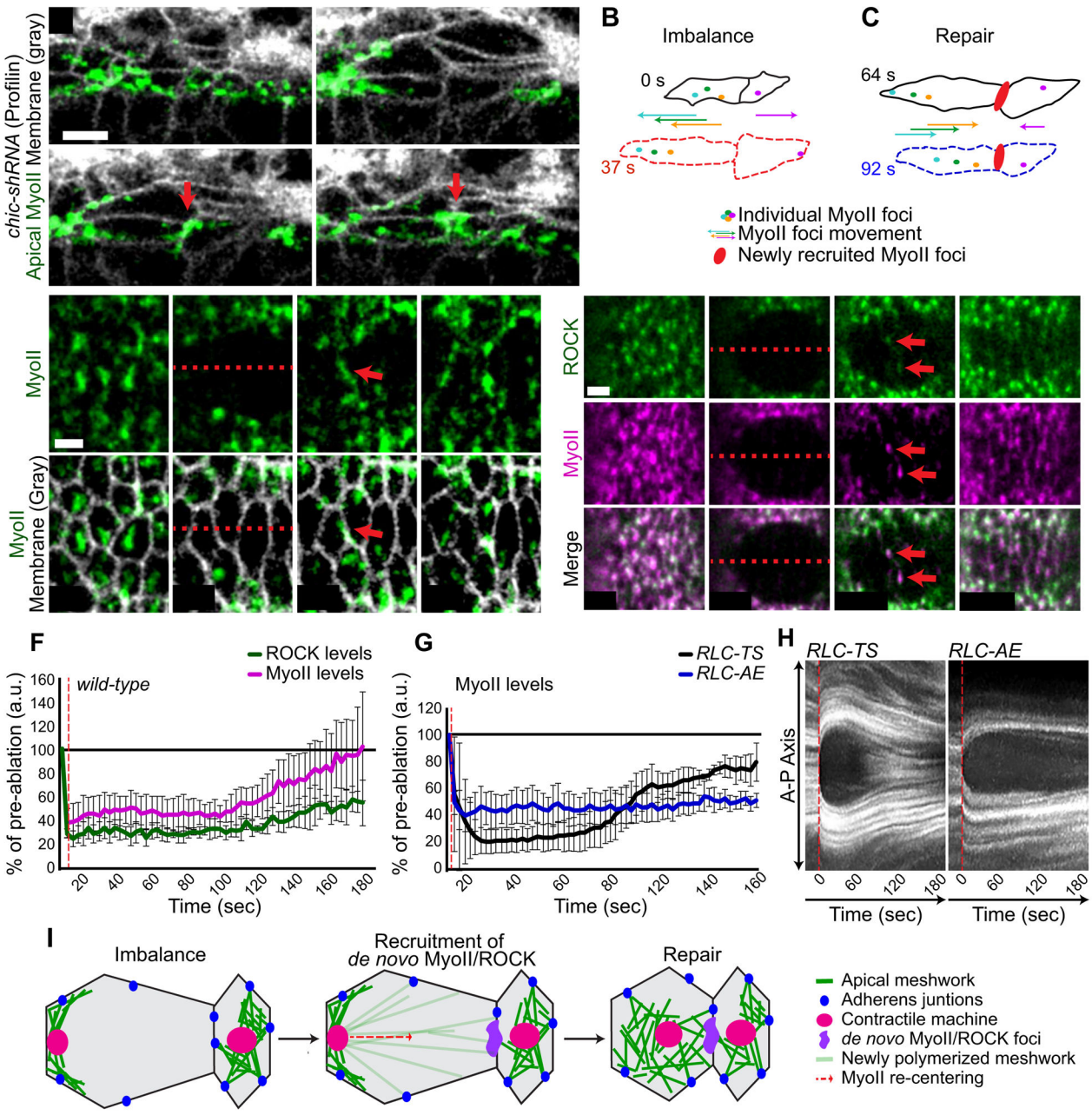

Figure 6. MyoII and ROCK are recruited to released junction

(A) Time-lapse images of *chic-shRNA* embryo expressing Sqh::GFP (MyoII), and Gap43::CHFP (membrane). Red arrow indicates *de novo* MyoII foci. (B and C) Schematic of cell outlines and MyoII structures (colored dots) corresponding with images in A. Representative images of live embryos expressing (D) Sqh::GFP (MyoII) and Gap43::CHFP (membrane) or (E) Sqh::CHFP (MyoII) and ubi-GFP::ROCK (ROCK) following mechanical severing of the contractile machinery attachment to junctions via laser ablation (red dotted line). (F) Average timing of the recruitment of indicated proteins to junction following mechanical ablation (red dotted line). n=4 embryos, 3 ROCK/MyoII foci per embryo. Error bars represent SEM. (G) Average timing of *wild-type* MyoII regulatory light chain (RLC-

TS) and phosphomutant regulatory light chain (RLC-AE; uncoupled from upstream signaling) recruitment to junction following laser ablation (red dotted line). n=3 embryos, ~5 MyoII foci per embryo for each condition. Error bars represent SEM. (H) Kymographs showing RLC-TS and RLC-AE recruitment to junction (red arrow) following laser ablation (red dotted line). (I) Schematic showing loss of force balance and repair process. MyoII and ROCK are recruited to the unattached cell-cell interface prior to the re-centering of MyoII and reestablishment of force balance (repair). See also Figure S5 and Movie S7.

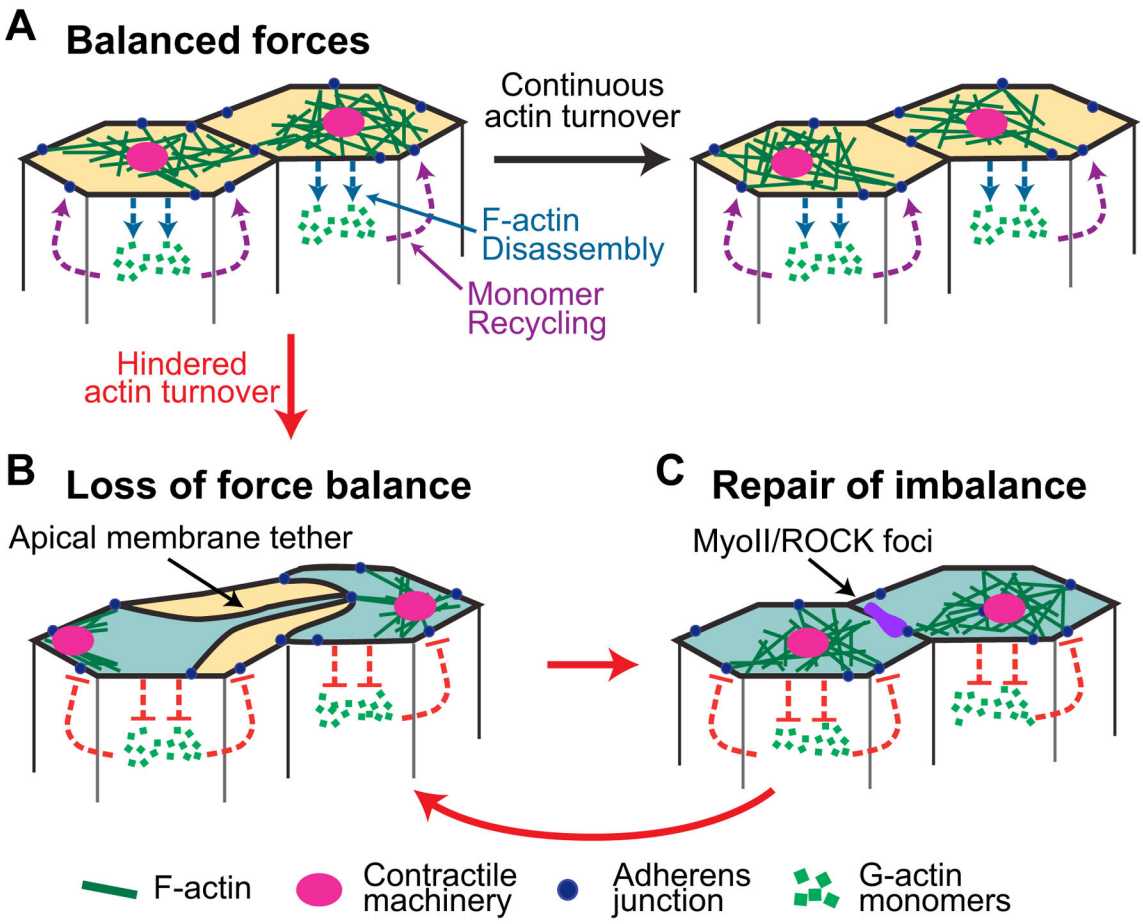

Figure 7. Model for proper attachment of the contractile machine to AJ

(A) Continuous F-actin turnover (blue and purple dotted lines) promotes dynamic reattachment of the contractile machinery to AJs during apical constriction. (B) Hindered F-actin turnover results in a separation of actomyosin meshworks, resulting from the contractile machine releasing one or more AJs and displacement of medioapical contractile machine. (C) MyoII/ROCK accumulates at the released junction and force balance is re-established. Loss of balance and repair occurs repeatedly (curved red arrow). See also Figure S6.